Topologically induced transparency in a two-phase metamaterial

Hafssaa Latioui, and Mário G. Silveirinha

Citation: Appl. Phys. Lett. **113**, 131106 (2018); doi: 10.1063/1.5042577
View online: https://doi.org/10.1063/1.5042577
View Table of Contents: http://aip.scitation.org/toc/apl/113/13
Published by the American Institute of Physics

Topologically induced transparency in a two-phase metamaterial

Hafssaa Latioui[1,2] and Mário G. Silveirinha[1,2,a)]
[1]*Department of Electrical Engineering, University of Coimbra, and Instituto de Telecomunicações, 3030-290 Coimbra, Portugal*
[2]*University of Lisbon–Instituto Superior Técnico - Avenida Rovisco Pais, 1, 1049-001 Lisboa, Portugal*

(Received 2 June 2018; accepted 11 August 2018; published online 27 September 2018)

It is theoretically and numerically demonstrated that a mixture of two topologically distinct material phases is characterized by an anomalous "transparency window" in a spectral range wherein the individual material phases are strongly reflecting. In particular, it is shown that a metamaterial formed by a metallic wire grid embedded in a magnetized plasma may support the propagation of waves with long wavelengths, notwithstanding the components, when taken separately, completely block the electromagnetic radiation. The effect is explained in terms of topological properties of the magnetoplasmon. Furthermore, it is highlighted that some naturally available materials may be regarded as a mixture of two topologically distinct phases, and hence may be characterized by a similar anomalous transparency effect as well. *Published by AIP Publishing*. https://doi.org/10.1063/1.5042577

Nonreciprocal effects in electromagnetic and nonreciprocal optical platforms have recently been the object of renewed interest and scrutiny, due to their unique and singular properties.[1–12] In particular, nonreciprocal systems enable one-way light flows and optical isolation.[2–4,8–12] Nonreciprocal effects are typically obtained by tailoring the permittivity or permeability response with a static magnetic field, but alternative solutions have been recently explored.[6–8,10,11,13,14]

Remarkably, some nonreciprocal systems have a topological nature.[15–22] Such systems are characterized by a topological integer that determines the number of topologically protected chiral edge states: the "Chern number." Indeed, the topology of a material can have remarkable consequences in the context of electromagnetic propagation: when a topological material is paired with another material with a trivial topology, unidirectional scattering-immune gapless edge states emerge in a common bulk bandgap, a result known as "the bulk edge correspondence" principle.[18,19,22,23] Furthermore, it was recently shown that the photonic Chern number has a precise physical meaning: it is the *quantum* of the light-angular momentum spectral density in a photonic insulator cavity.[23,24]

Building on these previous works, here, we theoretically demonstrate that topological edge modes (magneto-plasmons) may enable an anomalous "transparency effect" in a composite material formed by two topologically distinct fully-reflecting phases. We discuss how such an effect may be directly observed in naturally available materials and, in addition, propose a realistic physical implementation relying on the metamaterial concept. It is assumed that the electromagnetic fields have a time dependence of the form $e^{-i\omega t}$.

As a starting point, let us consider a mixture of two materials, characterized by the permittivity tensors $\bar{\varepsilon}_1$ and $\bar{\varepsilon}_2$, respectively. The effective permittivity of the mixture depends on the volume fraction of each material, the shape of the inclusions, lattice structure, etc.[25,26] As an illustration, for now, we use the simple mixing formula[27]

$$\bar{\varepsilon} \approx (1-f_V)\bar{\varepsilon}_1 + f_V\bar{\varepsilon}_2. \tag{1}$$

Here, f_V is the volume fraction of the 2nd material. Furthermore, we shall focus on the case $f_V \ll 1$, so that $\bar{\varepsilon} \approx \bar{\varepsilon}_1 + f_V(\bar{\varepsilon}_2 - \mathbf{1})$. It is supposed that the 1st material has a gyrotropic response, e.g., it may be a magnetized plasma characterized by the plasma frequency ω_p and the cyclotron frequency $\omega_c = -qB_0/m$ ($q = -e$ is the negative charge of the electrons, m is the effective mass and $\mathbf{B}_0 = B_0\hat{\mathbf{z}}$ is the bias magnetic field), for instance, a magnetized semiconductor.[28,29] Then, if the 2nd material is isotropic with a Drude dispersion ($\varepsilon_2 = 1 - \omega_{p2}^2/\omega^2$), it follows that the composite medium is characterized by a dielectric function of the form $\bar{\varepsilon} = \varepsilon_t\mathbf{1}_t + \varepsilon_a\hat{\mathbf{z}}\otimes\hat{\mathbf{z}} + i\varepsilon_g\hat{\mathbf{z}}\times\mathbf{1}$ ($\mathbf{1}_t = \mathbf{1} - \hat{\mathbf{z}}\otimes\hat{\mathbf{z}}$) with

$$\varepsilon_t = 1 - \frac{\omega_p^2}{\omega^2-\omega_c^2} - \frac{\tilde{\omega}_p^2}{\omega^2}, \quad \varepsilon_g = \frac{1}{\omega}\frac{\omega_p^2\omega_c}{\omega_c^2-\omega^2}, \tag{2}$$

and $\tilde{\omega}_p = \sqrt{f_V}\omega_{p2}$. The permittivity component ε_a is not relevant to this study, and hence is not shown. When $\tilde{\omega}_p = 0$, the permittivity tensor is coincident with that of the 1st material.[30] Magnetized plasmas and other gyrotropic media are generically topologically nontrivial materials.[20,22,31–33] On the other hand, the second material is reciprocal, and thus is topologically trivial. Hence, the global permittivity (2) models a composite formed by mixing two different topological phases; specifically, a mixture of a topologically nontrivial material (1st phase) and a topologically trivial material (2nd phase).

The dispersion relation of an electric gyrotropic bulk medium for transverse magnetic (TM) polarized waves [wave propagation in the xoy plane with $H = H_z(x,y)\hat{\mathbf{z}}$] is given by $k^2 = \varepsilon_{ef}(\omega/c)^2$, with $\varepsilon_{ef} = (\varepsilon_t^2 - \varepsilon_g^2)/\varepsilon_t$ being the equivalent permittivity of the gyrotropic material, $k^2 = k_x^2 + k_y^2$ and k_x, k_y the wave vector Cartesian components. Figure 1(a) shows the band diagram of the TM polarized

a)Author to whom correspondence should be addressed: mario.silveirinha@co.it.pt

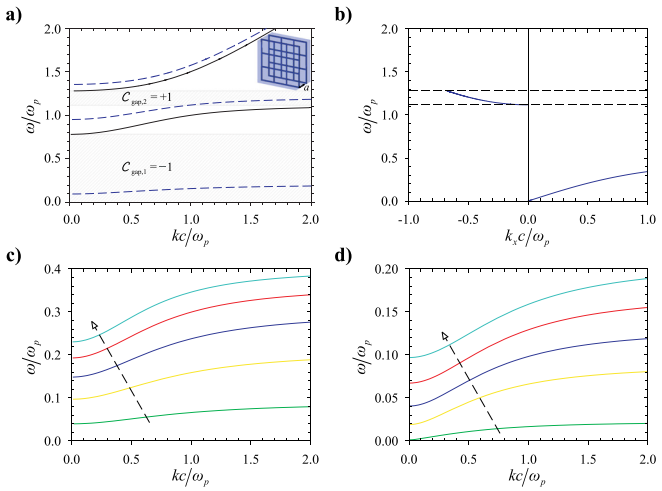

FIG. 1. (a) Band diagram of the composite material for propagation in the *xoy*-plane (TM-polarized waves) with $\omega_c = 0.5\omega_p$ for (i) $\alpha = 0$ (solid black lines) and (ii) $\alpha = 0.5$ (dashed blue lines). The inset depicts a possible metamaterial realization, with a stack of metallic wire grids embedded in a magnetized plasma. (b) Dispersion of the topological edge modes supported by a biased plasma ($\omega_c = 0.5\omega_p$ in the region $y > 0$) and a PEC interface ($y = 0$) for propagation along the *x*-direction. (c) Low frequency band for $\alpha = 0.5$ and $\omega_c/\omega_p = 0.2, 0.5, 0.8, 1.1, 1.4$ (the arrow indicates the direction of increasing ω_c/ω_p). (d) Low-frequency band for $\omega_c = 0.5\omega_p$ and $\alpha = 0.05, 0.2, 0.3, 0.4, 0.5$ (the arrow indicates the direction of increasing α).

plane waves for a composite medium with $\omega_c/\omega_p = 0.5$ and $\omega_{p2} = \omega_p$, so that $\tilde{\omega}_p = \alpha\omega_p$ with $\alpha = \sqrt{f_V}$ being determined by the volume fraction of the trivial material phase.

For $\alpha = 0$, the composite material has a single phase (1st component of the response) and the modes are organized in two branches. There are two photonic band-gaps highlighted as shaded regions in Fig. 1(a). The respective gap Chern numbers are found as explained in Refs. 20 and 21 and are given in the insets. The Chern numbers are nonzero, and hence the 1st phase is topologically nontrivial. On the other hand, the 2nd phase (with permittivity dispersion $\varepsilon_2 = 1 - \omega_{p2}^2/\omega^2$) has a topologically trivial low-frequency band-gap determined by $0 < \omega < \omega_{p2}$ (not shown).

Strikingly, for $\alpha = 0.5$ ($f_V = 0.25$), when the two different phases are mixed, a new low-frequency band ($0.10 < \omega/\omega_p < 0.21$) emerges well below the two relevant plasma frequencies (ω_p, ω_{p2}). This "transparency" window is the focus of our study. Figures 1(c) and 1(d) show how the transparency window changes under the variation of either ω_c/ω_p or α. Rather remarkably, the transparency window moves to even lower frequencies as either the volume fraction of the 2nd phase decreases (α decreases) or the bias magnetic field is reduced (lower values of ω_c/ω_p).

To demonstrate that the discovered low-frequency mode can be externally excited, next, we study the wave scattering by a slab of the two-phase topological material. It is assumed that the material slab is surrounded by air. The air interfaces are at $y = 0$ and $y = d$, so that the propagation is along the *y*-direction. The magnetic field can be written as:

$$H_z = H_0^{inc} e^{ik_x x} \times \begin{cases} e^{-\gamma_0 y} + Re^{+\gamma_0 y}, & y \le 0 \\ A_1 e^{-\gamma_g y} + A_2 e^{+\gamma_g y}, & 0 \le y \le d \\ Te^{-\gamma_0 (y-d)}, & y \ge d, \end{cases} \quad (3)$$

where $\gamma_0 = \sqrt{k_x^2 - (\omega/c)^2} = -i\sqrt{(\omega/c)^2 - k_x^2}$ and $\gamma_g = \sqrt{k_x^2 - \varepsilon_{ef}(\omega/c)^2}$, R and T are the reflection and transmission coefficients, H_0^{inc} is the amplitude of the incident wave, $k_x = (\omega/c)\sin\theta_i$, and θ_i is the angle of incidence. The electric field in the gyrotropic material can be found using $\mathbf{E} = \frac{1}{-i\omega\varepsilon_0}\bar{\varepsilon}^{-1} \cdot (\partial_y H_z \hat{\mathbf{x}} - \partial_x H_z \hat{\mathbf{y}})$ with $\bar{\varepsilon}^{-1} = \frac{1}{\varepsilon_{ef}}\left(\mathbf{1}_t - i\frac{\varepsilon_g}{\varepsilon_t}\hat{\mathbf{z}} \times \mathbf{1}_t\right) + \frac{1}{\varepsilon_a}\hat{\mathbf{z}} \otimes \hat{\mathbf{z}}$. Imposing the continuity of E_x and H_z at the interfaces, one can find the transmission and reflection coefficients and the A_1, A_2 coefficients. The dielectric function of the gyrotropic material is as in Eq. (2).

Figure 2(a) shows the amplitude of the transmission coefficient as a function of the normalized thickness $L\omega_p/c$ for $\omega_c/\omega_p = 0.5$, $\alpha = 0.5$ and different values of incidence angle. The frequency of operation is $\omega/\omega_p = 0.15$, and thus lies roughly in the middle of the low-frequency transparency window [see Fig. 1(a)]. As is seen, the transmission coefficient exhibits a rather standard behavior with transmission peaks at the Fabry-Pérot resonances. Curiously, the transmission level improves for oblique incidence. Furthermore, Fig. 2(b) shows the transmission coefficient as a function of the normalized frequency ω/ω_p for different values of the normalized thickness $L\omega_p/c$. Interestingly, independent of the slab thickness, the wave can tunnel through the two-phase material near the frequency $\omega/\omega_p \approx 0.1$, which determines the lower edge of the transparency window in Fig. 1(a). This property is reminiscent of the super-coupling effect characteristic of structures with near-zero refractive index.[34–36] As illustrated in Fig. 2(c), the transmission level is relatively robust to the effects of unavoidable material loss and remains larger than 0.5 at the first Fabry-Pérot resonance for a magnetized plasma with collision frequency $\Gamma/\omega_p = 0.015$.

Next, we discuss how to physically realize the proposed structure using the metamaterial concept. We suggest that the two-phase topological material may be implemented relying on a standard magnetized electron gas as the host medium (e.g., a magnetized doped semiconductor) and a metallic wire array. Evidently, the magnetized electron gas is expected to mimic the response of the nontrivial topological phase, whereas the wire array is expected to imitate the trivial topological phase. The wire medium is formed by a stack of 2D-metallic grids separated (along *z*) by the distance *a*[37,38] [see the inset of Fig. 1(a)]. Each metallic grid consists of two perpendicular co-planar arrays of metallic strips oriented along the *x* and *y* directions with period *a*. The width of the strips is $w = 0.1a$. For simplicity, the metal is modeled as a perfect electric conductor (PEC). By generalizing the homogenization approach of Refs. 37 and 39, we were able to demonstrate that the effective permittivity of the metamaterial approximately satisfies (neglecting spatially dispersive effects)

$$\bar{\varepsilon}_{ef} \approx \bar{\varepsilon}_h - \frac{c^2}{\omega^2}\beta_p^2 \mathbf{1}_t, \quad (4)$$

where $\bar{\varepsilon}_h$ is the relative permittivity of the gyrotropic host medium and $\beta_p \approx \frac{1}{a}(2\pi/(\ln(a/p) + 0.5275))^{1/2}$ with $p = 2w$ for strips with width w (for round metallic wires with radius r_w, one should instead use $p = 2\pi r_w$). Equation (4)

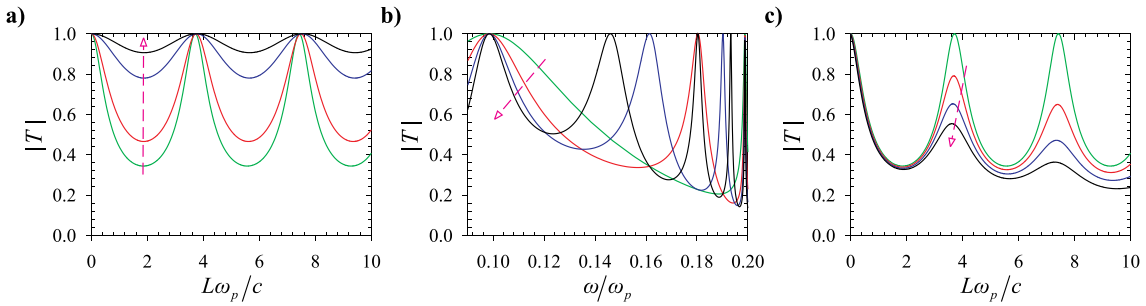

FIG. 2. (a) Amplitude of the transmission coefficient as a function of the normalized thickness $L\omega_p/c$ at the frequency $\omega = 0.15\omega_p$ for $\omega_c = 0.5\omega_p$ and $\alpha = 0.5$ and for the incidence angles: $\theta^{inc} = 0°, 45°, 70°, 80°$ (the arrow indicates the direction of increasing θ^{inc}). (b) Amplitude of the transmission coefficient as a function of ω/ω_p for $\omega_c = 0.5\omega_p$, $\alpha = 0.5$ and $\theta^{inc} = 0$ and for the normalized thicknesses: $L\omega_p/c = 1.0,\ 2.0,\ 3.0,\ 4.0$ (the arrow indicates the direction of increasing L). (c) Similar to (a) with $\theta^{inc} = 0°$ but for the plasma collision frequency: $\Gamma/\omega_p = 0,\ 0.005,\ 0.01,\ 0.015$ (the arrow indicates the direction of increasing Γ/ω_p).

extends the results of Ref. 37, 39, and 40 to a gyrotropic host material. Its detailed derivation will be reported elsewhere.

In our design, the host medium is taken as a magnetized plasma ($\omega_p/2\pi = 0.1$ THz) with a $+z$-directed magnetic bias with $\omega_c = 0.5\omega_p$. Interestingly, in this case, Eq. (4) reduces to Eq. (2) with $\tilde{\omega}_p = c\beta_p$. The unavoidable effect of loss is modeled by the collision frequency Γ. Here, we note that the inclusion of loss does not necessarily spoil the topological properties of the magnetized plasma.[41] The wire grid period was chosen as $a = 1.91$ mm. For $w = 0.1a$, one has $\beta_p \approx 1.7/a$, and therefore $\tilde{\omega}_p = \alpha\omega_p$ with $\alpha \approx 0.42$. Then, from Fig. 1(d), a new band is expected to emerge at $\omega \approx 0.073\omega_p$. In our simulations, the metamaterial slab is periodic along the x and z directions and has thickness L along the y direction. We chose a periodic array of short horizontal electric dipoles (oriented along the x-direction) as the excitation. The dipole array emits a plane wave that illuminates the metamaterial slab along the normal direction.

Figure 3(a) (black symbols) shows that similar to the continuum model, the metamaterial structure enables an anomalous wave tunneling at very low frequencies ($\omega = 0.095\omega_p$), where one would expect the electron gas and the wire grid to completely block the wave propagation. The effect occurs even in the presence of realistic loss values ($\Gamma = 0.1\omega_p$). However, the transmission level with metamaterial realization is weaker than in Fig. 2, in part due to the larger values of Γ and in part due to spatial dispersion effects that are not captured by Eq. (4). The matching between the metamaterial slab and the air regions can be noticeably improved with quarter-wavelength transformers at the input and output interfaces [blue symbols in Fig. 3(a)]. In this case, the transmission amplitude may reach 15% for the thickness $L = 3a$. Figure 3(b) shows that the transmission level depends significantly on the thickness, due to the excitation of Fabry-Pérot resonances, further supporting that the metamaterial really supports a propagating mode.

Figure 3(c) shows a time snapshot of the magnetic field at the frequency $\omega = 0.095\omega_p$ and for a thickness $L = 5a$. The time animation of the fields is available in the supplementary material and reveals that in each metal loop the wave follows a rotating motion, such that the energy tends to circulate in closed orbits and the fields have a nontrivial angular momentum.[24,31] This property can be understood as a consequence of the excitation of topological edge modes (magneto-plasmons) at the wire grid-gyrotropic material interface, due to the different topological nature of the two material phases. The dispersion of the magneto-plasmon mode is depicted in Fig. 1(b) for the case of a planar interface ($y = 0$) between the gyrotropic host material and a PEC. The edge mode dispersion is found as explained in Refs. 9, 20, and 22. As is seen, the low-frequency unidirectional edge mode propagates exclusively towards the $+x$-direction in the spectral range $0 < \omega < \omega_c$. When the gyrotropic material fills a closed metallic cavity, the low-frequency edge-mode will go around the cavity walls following an anti-clockwise motion,[24] consistent with the winding motion of the magneto-plasmons in each loop of the wire grid. Thus, the anomalous transparency effect can be understood as a consequence of the excitation of topological modes that create coupled vortices of the electromagnetic field [see Fig. 3(c)

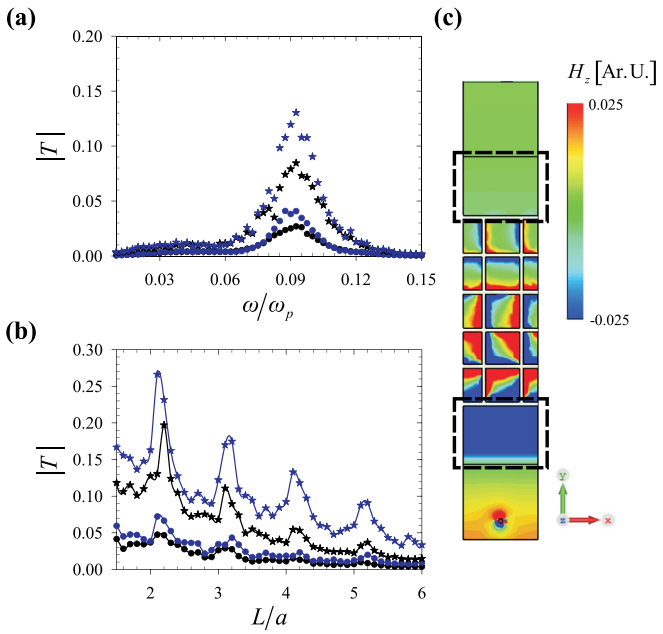

FIG. 3. (a) Amplitude of the transmission coefficient as a function of the normalized frequency ω/ω_p for $\omega_p/(2\pi) = 0.1$ THz, $\omega_c = 0.5\omega_p$, $a = 1.91$ mm, $\theta^{inc} = 0$, and $L = 3a$ for $\Gamma = 0.1\omega_p$ (black symbols) and for $\Gamma = 0.05\omega_p$ (blue symbols), without impedance transformers (circle symbols) and with $\lambda/4$ transformers with $\varepsilon_{trans} = 6.7$ (star symbols). (b) Amplitude of the transmission coefficient as a function of the normalized thickness L/a at the frequency $\omega = 0.095\omega_p$. The legend and the remaining structural parameters are as in (a). (c) Time snapshot of the magnetic field (H_z) emitted by the dipole array at the frequency $\omega = 0.095\omega_p$, for $L = 5a$, $\Gamma = 0.1\omega_p$, and $\varepsilon_{trans} = 6.7$. The remaining structural parameters are the same as in panel (a). The black dashed rectangles indicate the location of the $\lambda/4$ transformers. The results are obtained with a full wave simulator.[42]

and the time animation in the supplementary material]. Indeed, due to the different Chern numbers of the bulk materials, the bulk-edge correspondence indicates that localized surface states may emerge on metal structures embedded in a gyrotropic material (strictly speaking, the bulk edge correspondence can be applied to planar interfaces, and hence the argument is semi-heuristic). The "transparency band" is due to the near-field coupling of the states supported by different cells.

Incidentally, some naturally available materials may be as well regarded as a mixture of two inequivalent topological phases with features analogous to those of the model of Eq. (2). For example, let us consider a situation where the microscopic drift current of a plasma is dictated by two species of current carriers (e.g., with different effective masses or different densities), i.e., the electron gas is formed by two distinct current "channels." Each species of carriers reacts differently to a bias field, and thereby the combined response of the two-channels may yield the different terms of the dielectric function (2). An illustration of this concept is provided by standard semiconductors, for example, GaAs. The dielectric function of GaAs has three contributions: (i) the bound charges, (ii) the free electrons and (iii) the electrons-holes. The response of the bound charges is insensitive to a bias magnetic field and may be described by a static permittivity term, $\varepsilon_s = 12.8$. On the other hand, both the electrons and the holes originate drift-currents, yielding a multi-component plasma. The dielectric function of GaAs is of the form

$$\varepsilon_t = \varepsilon_s - \frac{\omega_{pe}^2}{\omega^2 - \omega_{ce}^2} - \frac{\omega_{ph}^2}{\omega^2 - \omega_{ch}^2},$$
$$\varepsilon_g = \frac{1}{\omega}\frac{\omega_{pe}^2\omega_{ce}}{\omega_{ce}^2 - \omega^2} + \frac{1}{\omega}\frac{\omega_{ph}^2\omega_{ch}}{\omega_{ch}^2 - \omega^2}, \tag{5}$$

with ω_{pe} and ω_{ph} (ω_{ce} and ω_{ch}) being the plasma (cyclotron) frequencies for electrons and holes. Interestingly, comparing with Eq. (1), one sees that the dielectric function of the semiconductor is the same as the one for a mixture of two gyrotropic materials with parameters $(\omega_{pe}, \omega_{ce})$ and $(\omega_{ph}, \omega_{ch})$. For GaAs, the effective masses of electrons and holes are related as $m_e^* = 0.134 m_h^*$.[43,44] Hence, the cyclotron frequencies of the two species are linked as $\omega_{ch} = -0.134\omega_{ce}$, and hence have *opposite signs*. Since the sign of the gap Chern number is linked to the sign of the cyclotron frequency,[20,21] the material phases determined by each of the current carriers (electrons or holes) are topologically inequivalent. Indeed, for a $+z$-directed bias magnetic field, the band structure determined by the gyrotropic response with parameters ω_{pe}, ω_{ce} $(\omega_{ph}, \omega_{ch})$ has a low-frequency band-gap with the gap Chern number being -1 $(+1)$.

Figure 4(a) shows the band diagram of GaAs with and without a bias magnetic field. The plasma frequency $(\omega_p = (e^2 n/\varepsilon_0 m^*)^{1/2})$ depends on the concentration (n) and the effective mass (m^*) of each carrier species. For an intrinsic semiconductor, the concentration of electrons and holes is identical, and for the GaAs case, $\omega_{ph} = 0.37\omega_{pe}$. As is seen, when $\omega_{ce} = 0 = \omega_{ch}$ (unbiased semiconductor) the dispersion of the modes [black solid line in Fig. 4(a); the flat band associated with longitudinal modes is not shown] has a

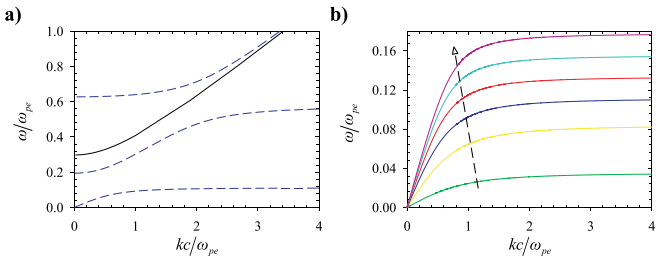

FIG. 4. Band diagram of GaAs for propagation in the xoy-plane. (a) Unbiased (black solid line) and biased (blue dashed lines) GaAs with $\omega_{ce}/\omega_{pe} = 0.5$. (b) The low frequency band for different values of the field bias $\omega_{ce}/\omega_{pe} = 0.1, 0.3, 0.5, 0.7, 0.9, 1.1$ (the arrow indicates the direction of increasing ω_{ce}/ω_{pe}).

single band-gap defined by $0 < \omega < \omega_U \approx \omega_{pe}/\sqrt{\varepsilon_s}$. Note that without the bias magnetic field, both the electron and hole phases are trivial. In contrast, with a bias magnetic field, the electron and hole phases become topologically distinct due to the different signs of cyclotron frequencies. Hence, similar to the permittivity model (2), the combination of the two distinct topologically phases (which can be observed simply by applying a static bias magnetic field) determines the emergence of a low-frequency transparency window. The transparency window moves to lower frequencies as the bias magnetic field is reduced (ω_{ce}/ω_{pe} decreases), as shown in Fig. 4(b), analogous to Fig. 1(d). It is interesting to note that the "electrons" and "holes" determine two independent current channels, somewhat analogous to the metamaterial design wherein the two material components (metal and magnetized plasma) also determine different paths for the electric current.

In summary, we theoretically demonstrated that by mixing two distinct topological material phases it is possible to create unusual conditions for wave propagation in a spectral range wherein the two phases are impenetrable by light. An electron gas with two current channels (e.g., intrinsic semiconductors) may provide an ideal platform to realize such a structure. In addition, we proposed a realistic metamaterial implementation of the suggested system. Detailed numerical simulations confirm that a material with two distinct topological phases enables, indeed, an anomalous wave tunneling at extremely low frequencies, and thus opens new inroads and opportunities for topological effects in the terahertz and microwave ranges.

See supplementary material for the time animation of Fig. 3(c).

This work was supported in part by Fundação para a Ciência e a Tecnologia with Grant Nos. PTDC/EEITEL/4543/2014 and UID/EEA/50008/2017.

[1]A. Figotin and I. Vitebsky, "Nonreciprocal magnetic photonic crystals," Phys. Rev. E **63**, 066609 (2001).
[2]Z. Wang, Y. D. Chong, J. D. Joannopoulos, and M. Soljačić, "Refection-free one-way edge modes in a gyromagnetic photonic crystal," Phys. Rev. Lett. **100**, 013905 (2008).
[3]Z. Yu, G. Veronis, Z. Wang, and S. Fan, "One-way electromagnetic waveguide formed at the interface between a plasmonic metal under a static magnetic field and a photonic crystal," Phys. Rev. Lett. **100**, 023902 (2008).

[4]K. Fang, Z. Yu, V. Liu, and S. Fan, "Ultracompact nonreciprocal optical isolator based on guided resonance in a magneto-optical photonic crystal slab," Opt. Lett. **36**, 4254–4256 (2011).
[5]D. L. Sounas and C. Caloz, "Gyrotropy and nonreciprocity of graphene for microwave applications," IEEE Trans. Microwave Theory Tech. **60**, 901 (2012).
[6]T. Kodera, D. L. Sounas, and C. Caloz, "Artificial Faraday rotation using a ring metamaterial structure without static magnetic field," Appl. Phys. Lett. **99**, 031114 (2011).
[7]D. L. Sounas, T. Kodera, and C. Caloz, "Electromagnetic modeling of a magnetless and nonreciprocal gyrotropic metasurface," IEEE Trans. Antennas Propag. **61**, 221–231 (2013).
[8]Z. Yu and S. Fan, "Complete optical isolation created by indirect interband photonic transitions," Nat. Photonics **3**, 91–94 (2009).
[9]A. R. Davoyan and N. Engheta, "Theory of wave propagation in magnetized near-zero-epsilon metamaterials: Evidence for one-way photonic states and magnetically switched transparency and opacity," Phys. Rev. Lett. **111**, 257401 (2013).
[10]A. M. Mahmoud, A. R. Davoyan, and N. Engheta, "All-passive nonreciprocal metastructure," Nat. Commun. **6**, 8359 (2015).
[11]F. R. Prudêncio and M. G. Silveirinha, "Optical isolation of circularly polarized light with a spontaneous magnetoelectric effect," Phys. Rev. A **93**, 043846 (2016).
[12]M. G. Silveirinha, "PTD symmetry protected scattering anomaly in optics," Phys. Rev. B **95**, 035153 (2017).
[13]D. L. Sounas and A. Alù, "Non-reciprocal photonics based on time modulation," Nat. Photonics **11**, 774 (2017).
[14]T. A. Morgado and M. G. Silveirinha, "Drift-induced unidirectional graphene plasmons," e-print arXiv:1711.08367.
[15]F. D. M. Haldane and S. Raghu, "Possible realization of directional optical waveguides in photonic crystals with broken time-reversal symmetry," Phys. Rev. Lett. **100**, 013904 (2008).
[16]Z. Wang, Y. Chong, J. D. Joannopoulos, and M. Soljačić, "Observation of unidirectional backscattering immune topological electromagnetic states," Nature **461**, 772 (2009).
[17]D. Jin, L. Lu, Z. Wang, C. Fang, J. D. Joannopoulos, M. Soljacic, L. Fu, and N. X. Fang, "Topological magnetoplasmon," Nat. Commun. **7**, 13486 (2016).
[18]L. Lu, J. D. Joannopoulos, and M. Soljačić, "Topological photonics," Nat. Photonics **8**, 821 (2014).
[19]T. Ozawa, H. M. Price, A. Amo, N. Goldman, M. Hafezi, L. Lu, M. C. Rechtsman, D. Schuster, J. Simon, O. Zilberberg, and I. Carusotto, "Topological photonics," preprint arXiv:1802.04173 (2018).
[20]M. G. Silveirinha, "Chern invariants for continuous media," Phys. Rev. B **92**, 125153 (2015).
[21]M. G. Silveirinha, "Topological classification of Chern-type insulators by means of the photonic Green function," Phys. Rev. B **97**, 115146 (2018).
[22]M. G. Silveirinha, "Bulk edge correspondence for topological photonic continua," Phys. Rev. B **94**, 205105 (2016).
[23]M. G. Silveirinha, "Proof of the bulk-edge correspondence through a link between topological photonics and fluctuation-electrodynamics," preprint arXiv:1804.02190 (2018).
[24]M. G. Silveirinha, "Quantized angular momentum in topological optical systems," preprint arXiv:1803.07121 (2018).
[25]M. G. Silveirinha, "A metamaterial homogenization approach with application to the characterization of microstructured composites with negative parameters," Phys. Rev. B **75**, 115104 (2007).
[26]M. Xiao and S. Fan, "Photonic Chern insulator through homogenization of an array of particles," Phys. Rev. B **96**, 100202(R) (2017).
[27]A. H. Sihvola, *Electromagnetic Mixing Formulas and Applications* (IET, London, 1999).
[28]E. D. Palik, R. Kaplan, R. W. Gammon, H. Kaplan, R. F. Wallis, and J. J. Quinn II, "Coupled surface magnetoplasmon-optic-phonon polariton modes on InSb," Phys. Rev. B **13**, 2497 (1976).
[29]E. Moncada-Villa, V. Fernández-Hurtado, F. J. García-Vidal, A. García-Martín, and J. C. Cuevas, "Magnetic field control of near-field radiative heat transfer and the realization of highly tunable hyperbolic thermal emitters," Phys. Rev. B **92**, 125418 (2015).
[30]J. A. Bittencourt, *Fundamentals of Plasma Physics*, 3rd ed. (Springer-Verlag, NY, 2010).
[31]M. G. Silveirinha, "Topological angular momentum and radiative heat transport in closed orbits," Phys. Rev. B **95**, 115103 (2017).
[32]S. A. H. Gangaraj, A. Nemilentsau, and G. W. Hanson, "The effects of three-dimensional defects on one-way surface plasmon propagation for photonic topological insulators comprised of continuum media," Sci. Rep. **6**, 30055 (2016).
[33]S. A. H. Gangaraj and G. W. Hanson, "Topologically protected unidirectional surface states in biased ferrites: Duality and application to directional couplers," IEEE Antennas Wireless Propag. Lett. **16**, 449 (2016).
[34]M. Silveirinha and N. Engheta, "Tunneling of electromagnetic energy through sub-wavelength channels and bends using near-zero-epsilon materials," Phys. Rev. Lett. **97**, 157403 (2006).
[35]M. G. Silveirinha and N. Engheta, "Theory of supercoupling, squeezing wave energy, and field confinement in narrow channels and tight bends using epsilon-near-zero metamaterials," Phys. Rev. B **76**, 245109 (2007).
[36]N. Engheta, "Pursuing near-zero response," Science **340**, 286–287 (2013).
[37]M. G. Silveirinha and C. A. Fernandes, "Homogenization of 3D- connected and non-connected wire metamaterials," IEEE Trans. Microwave Theory Tech. **53**, 1418 (2005).
[38]M. G. Silveirinha and C. A. Fernandes, "Transverse average field approach for the characterization of thin metamaterial slabs," Phys. Rev. E **75**, 036613 (2007).
[39]M. G. Silveirinha, "Artificial plasma formed by connected metallic wires at infrared frequencies," Phys. Rev. B **79**, 035118 (2009).
[40]P. A. Belov, R. Marqués, S. I. Maslovski, I. S. Nefedov, M. Silveirinha, C. R. Simovsky, and S. A. Tretyakov, "Strong spatial dispersion in wire media in the very large wavelength limit," Phys. Rev. B **67**, 113103 (2003).
[41]H. Shen, B. Zhen, and L. Fu, "Topological band theory for non-Hermitian Hamiltonians," Phys. Rev. Lett. **120**, 146402 (2018).
[42]CST Microwave Studio, http://www.cst.com for information about the electromagnetic simulator (2017).
[43]M. R. Amin, "Quantum effects on compressional Alfven waves in compensated semiconductors," Phys. Plasmas **22**, 032303 (2015).
[44]A. Moradi, "Surface and bulk plasmons of electron-hole plasma in semiconductor nanowires," Phys. Plasmas **23**, 114503 (2016).